Beam Test 2009 – Properties, Comparability, Resolution Limits, and Comparison to Digitizer Predictions

Christian Geisler, Benjamin Schwenker

II. Institute
Atomic and Nuclear Physics
University of Göttingen

5th International Workshop on DEPFET Detectors and Applications
September 2010

GEORG-AUGUST-UNIVERSITÄT
GÖTTINGEN

VolkswagenStiftung

DUT in Beam Test 2009

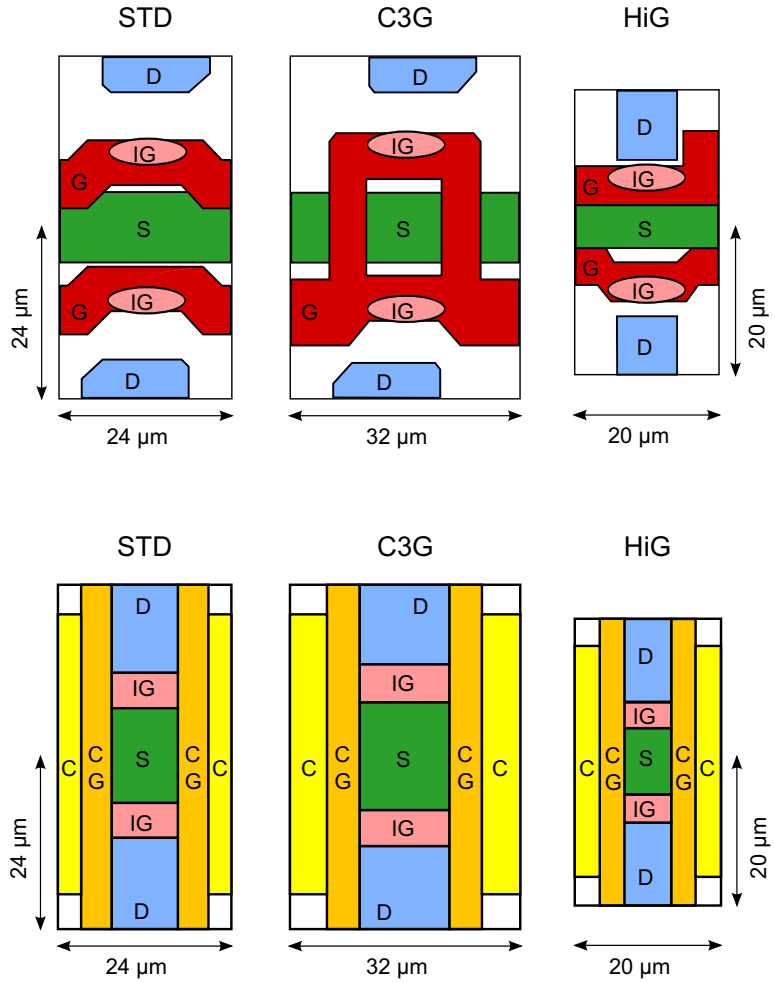

Figure: Layout of the metallization layer (top) and the implantation zones (bottom) of the double-pixel structures. Shown are the source (S), gate (G) and drain (D) contacts of the FET structure as well as the approximate position of the internal gate (IG). The metal contacts of the clear region (C) and clear gate (CG) are not shown.

Internal Gain, Charge Collection Efficiency, and Large Scale Homogeneity

DUT	S_P	$g_q^{S_P}$	$Min(\langle S \rangle)$	$\langle\langle S \rangle\rangle$	$Max(\langle S \rangle)$	dir.	RMS_{adj}
STD	1791±10	379±15	1860	1920 ± 14	1960	x	$1.5\% \pm 0.4\%$
						y	$1.0\% \pm 1.0\%$
C3G	2437±10	516±21	2900	2940 ± 36	2990	x	$1.6\% \pm 0.8\%$
						y	$4.0\% \pm 2.2\%$
HiG	3246±10	688±27	3410	3480 ± 45	3530	x	$1.0\% \pm 0.7\%$
						y	$1.7\% \pm 1.8\%$

Table: MPV of cluster signal S_P [ADC counts], internal gain $g_g^{S_P}$ [nA/e$^-$], minimal, average and maximal in-pixel cluster signal $\langle S \rangle$ [ADC counts], and RMS spread of difference of internal gains of adjacent pixels in x and y RMS_{adj}.

Internal Gain, Charge Collection Efficiency, and Large Scale Homogeneity

DUT	S_P	$g_q^{S_P}$	$Min(\langle S \rangle)$	$\langle\langle S \rangle\rangle$	$Max(\langle S \rangle)$	dir.	RMS_{adj}
STD	1791±10	379±15	1860	1920 ± 14	1960	x	$1.5\% \pm 0.4\%$
						y	$1.0\% \pm 1.0\%$
C3G	2437±10	516±21	2900	2940 ± 36	2990	x	$1.6\% \pm 0.8\%$
						y	$4.0\% \pm 2.2\%$
HiG	3246±10	688±27	3410	3480 ± 45	3530	x	$1.0\% \pm 0.7\%$
						y	$1.7\% \pm 1.8\%$

Table: MPV of cluster signal S_P [ADC counts], internal gain $g_g^{S_P}$ [nA/e$^-$], minimal, average and maximal in-pixel cluster signal $\langle S \rangle$ [ADC counts], and RMS spread of difference of internal gains of adjacent pixels in x and y RMS_{adj}.

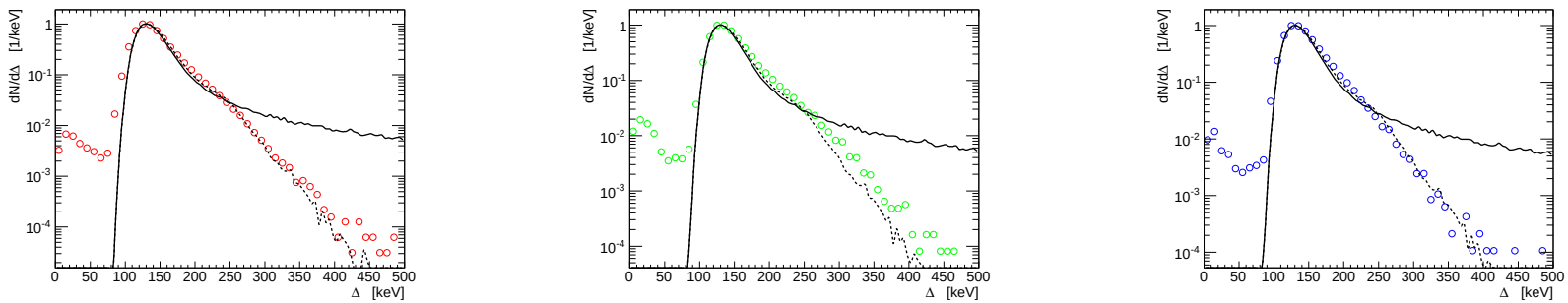

Figure: Measured energy straggling in DUT (l.t.r. STD, C3G, HiG) (circles) in comparison to the calculated $F(\Delta)$ (solid line) and the empirically altered $F'(\Delta)$ (dotted line).

Internal Gain, Charge Collection Efficiency, and Large Scale Homogeneity

DUT	S_P	$g_q^{S_P}$	$Min(\langle S \rangle)$	$\langle\langle S \rangle\rangle$	$Max(\langle S \rangle)$	dir.	RMS_{adj}
STD	1791±10	379±15	1860	1920 ± 14	1960	x	$1.5\% \pm 0.4\%$
						y	$1.0\% \pm 1.0\%$
C3G	2437±10	516±21	2900	2940 ± 36	2990	x	$1.6\% \pm 0.8\%$
						y	$4.0\% \pm 2.2\%$
HiG	3246±10	688±27	3410	3480 ± 45	3530	x	$1.0\% \pm 0.7\%$
						y	$1.7\% \pm 1.8\%$

Table: MPV of cluster signal S_P [ADC counts], internal gain $g_g^{S_P}$ [nA/e$^-$], minimal, average and maximal in-pixel cluster signal $\langle S \rangle$ [ADC counts], and RMS spread of difference of internal gains of adjacent pixels in x and y RMS_{adj}.

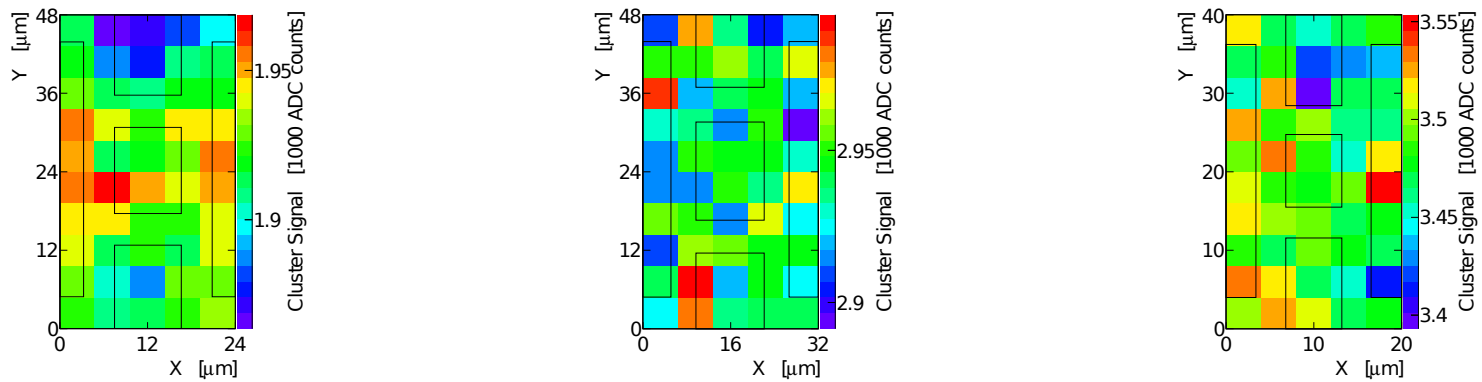

Figure: Total cluster charge in dependence on the in-pixel point of passage (x, y) through a double-pixel of the DUT (l.t.r. STD, C3G, HiG). A 6% fluctuation between the drain and clear region is apparent in the STD. On the other devices the fluctuation is not significant and could be caused by the limited statistics. Overlaid are the outlines of the gate structures.

Internal Gain, Charge Collection Efficiency, and Large Scale Homogeneity

DUT	S_P	$g_q^{S_P}$	$Min(\langle S \rangle)$	$\langle\langle S \rangle\rangle$	$Max(\langle S \rangle)$	dir.	RMS_{adj}
STD	1791±10	379±15	1860	1920 ± 14	1960	x	$1.5\% \pm 0.4\%$
						y	$1.0\% \pm 1.0\%$
C3G	2437±10	516±21	2900	2940 ± 36	2990	x	$1.6\% \pm 0.8\%$
						y	$4.0\% \pm 2.2\%$
HiG	3246±10	688±27	3410	3480 ± 45	3530	x	$1.0\% \pm 0.7\%$
						y	$1.7\% \pm 1.8\%$

Table: MPV of cluster signal S_P [ADC counts], internal gain $g_g^{S_P}$ [nA/e$^-$], minimal, average and maximal in-pixel cluster signal $\langle S \rangle$ [ADC counts], and RMS spread of difference of internal gains of adjacent pixels in x and y RMS_{adj}.

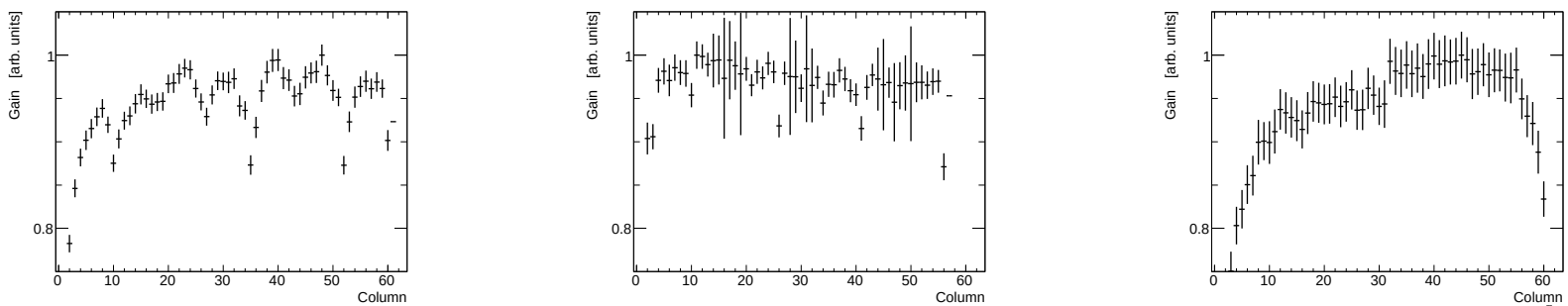

Figure: X – gain modulation of DUT (l.t.r. STD, C3G, HiG) of TB2009. The gain has been calculated as the row and column-wise averaged seed signal. The scale is set to unity at the highest value.

Internal Gain, Charge Collection Efficiency, and Large Scale Homogeneity

DUT	S_P	$g_q^{S_P}$	$Min(\langle S \rangle)$	$\langle\langle S \rangle\rangle$	$Max(\langle S \rangle)$	dir.	RMS_{adj}
STD	1791±10	379±15	1860	1920 ± 14	1960	x	$1.5\% \pm 0.4\%$
						y	$1.0\% \pm 1.0\%$
C3G	2437±10	516±21	2900	2940 ± 36	2990	x	$1.6\% \pm 0.8\%$
						y	$4.0\% \pm 2.2\%$
HiG	3246±10	688±27	3410	3480 ± 45	3530	x	$1.0\% \pm 0.7\%$
						y	$1.7\% \pm 1.8\%$

Table: MPV of cluster signal S_P [ADC counts], internal gain $g_g^{S_P}$ [nA/e$^-$], minimal, average and maximal in-pixel cluster signal $\langle S \rangle$ [ADC counts], and RMS spread of difference of internal gains of adjacent pixels in x and y RMS_{adj}.

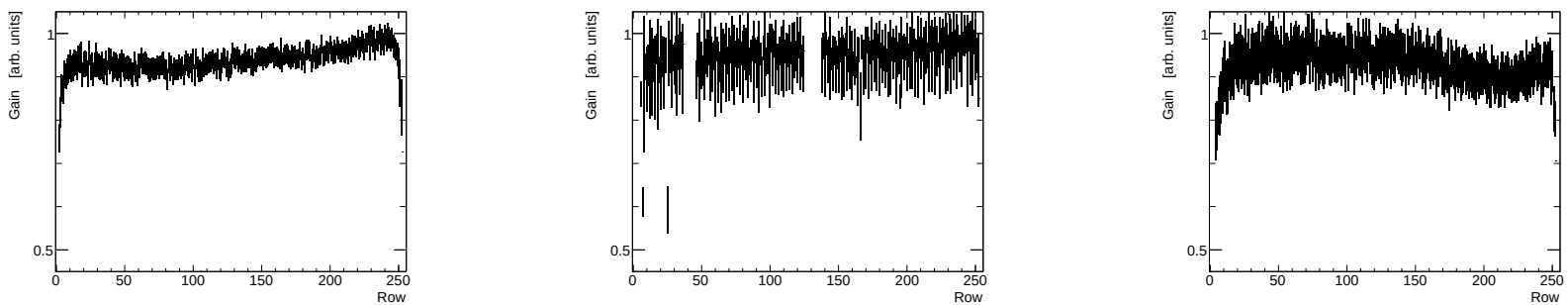

Figure: Y – gain modulation of DUT (l.t.r. STD, C3G, HiG) of TB2009. The gain has been calculated as the row and column-wise averaged seed signal. The scale is set to unity at the highest value.

Findings to be Published

"Charge Collection Paper"

- Noise of detector and readout chain (ENC)
- Internal gain of different prototypes (measurements from TB and Am-source)
- Gain variation
- Edge Effect and Large Scale inhomogeneities
- In-Pixel inhomogeneities
- Voltage Scan

"Resolution Paper"

- In-pixel residuals / resolution

Edge Effect and Large Scale Response

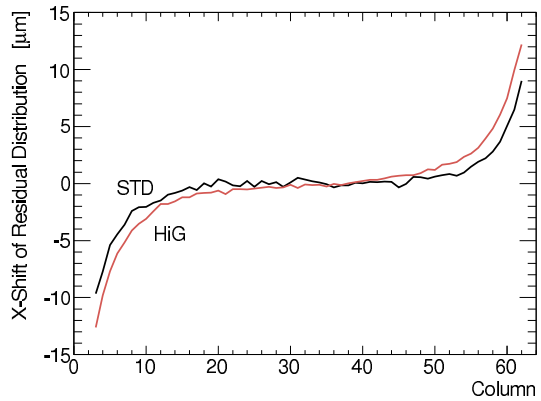

(a) Edge effect in x.

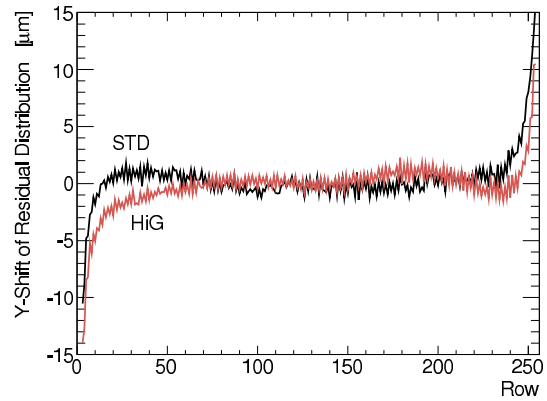

(b) Edge effect in y.

Figure 6.13: Shifted position reconstruction in x and y direction for STD and HiG.

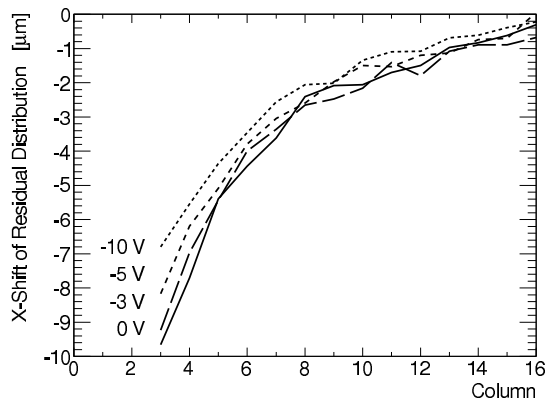

(a) Edge effect in first columns in x.

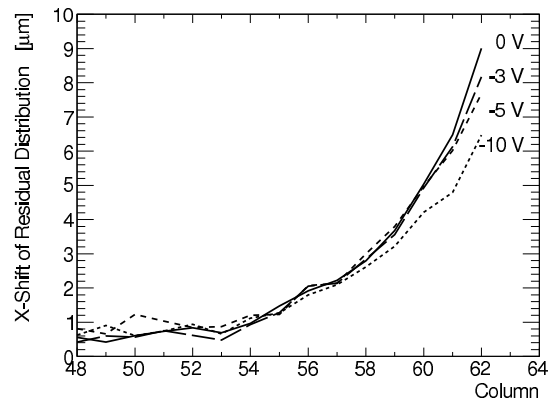

(b) Edge effect in last columns in x.

Figure 6.15: Effect of different edge ring voltages on systematic shift of position reconstruction on STD DUT.

Comparison of Residuals and Resolution Limits

Device	dir.	σ_G	σ_P
Mod 11	x	2.39	2.49
	y	2.24	2.28
Mod 4	x	1.52	1.60
	y	1.27	1.38
HiG	x	1.46	1.54
	y	1.42	1.42
Mod 8	x	1.81	1.98
	y	1.55	1.61
Mod 9	x	1.97	1.97
	y	1.60	1.61
Mod 5	x	2.86	3.24
	y	2.89	2.86

Table: Results from fitting a Gaussian (μ, σ) (range: $\pm 10 \mu m$) to the unbiased residual distributions of all sensors in run 2285. The σ_G values are the results of the analysis presented here and σ_P are the results of the analysis performed by Kodyš et al. All values are in units of μm.

DUT	dir.	Δd_l	Δd	Δd_u
STD	x	0.73	1.19 ± 0.16	1.38
	y	0.84	1.39 ± 0.06	1.46
C3G	x	1.23	1.55 ± 0.13	1.70
	y	1.03	1.51 ± 0.06	1.58
HiG	x	0.40	1.03 ± 0.19	1.24
	y	0.77	1.34 ± 0.07	1.42

Table: Resolution estimates for the DUT. The resolution is calculated for the average, upper and lower limit of telescope sensor resolution. All values are in units of μm.

Test Beam and Monte Carlo Setup

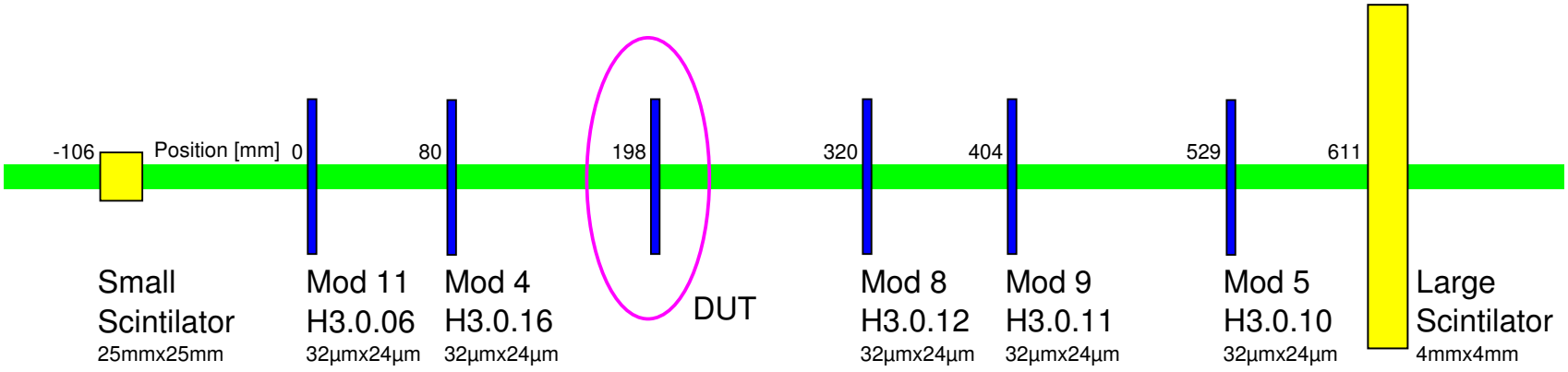

Test beam setup at CERN SPS 2009 (120 GeV pions)

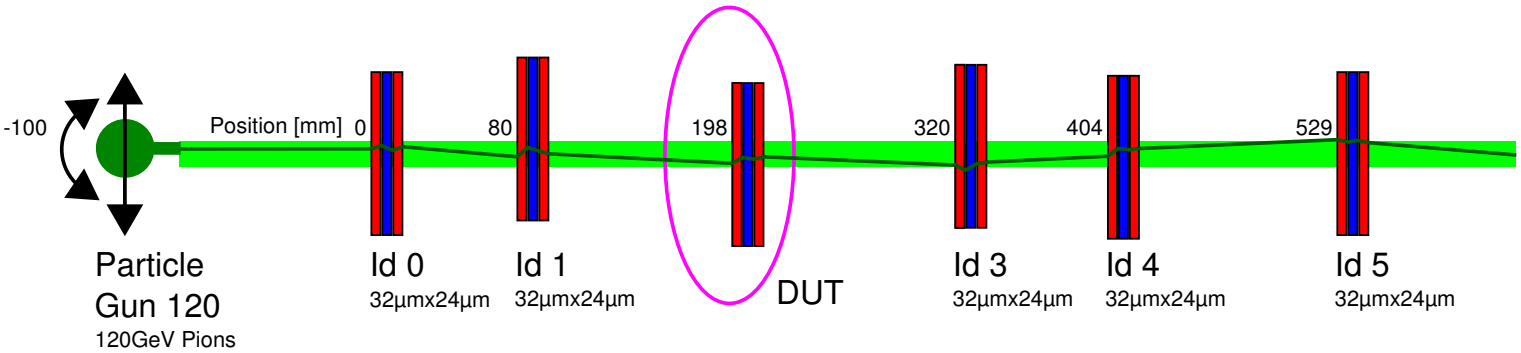

Geometry for MC validation studies

In Pixel Residual and Comparison to Digitizer

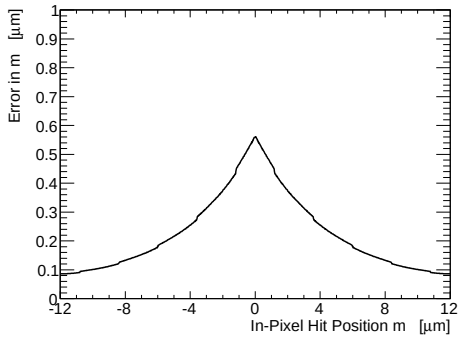

Figure: Analytical calculation of in-pixel resolution with toy-model. Input: Pixel Pitch, Diffusion, and S/N.

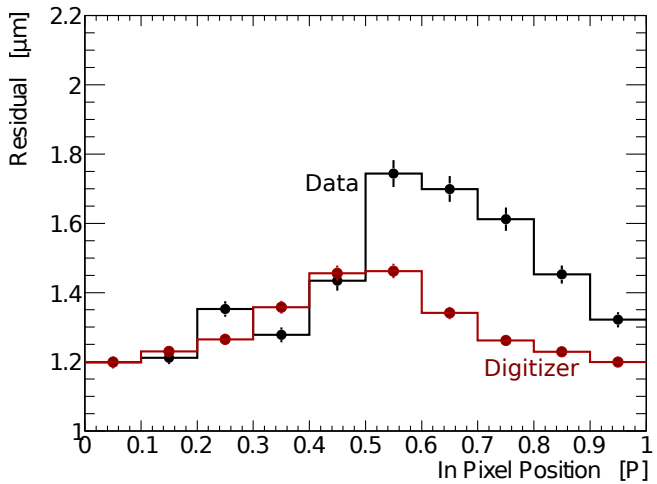

Figure: In-Pixel residual of Data and Digitizer (x, STD).

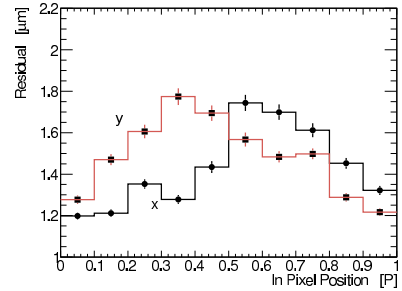

(a) STD

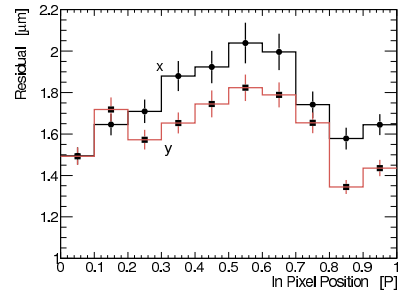

(b) C3G

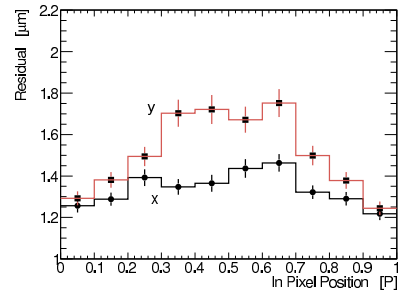

(c) HiG

Figure 6.19: Unbiased residuals in x (black) and y (red) in dependence on the in-pixel point of passage m through the DUT. The residual is largest in the center region of the pixel where the charge sharing and thus the S/N of the η value is minimal. The variation of the residual (and consequently the resolution) with m is an intrinsic property of a segmented detector and the reconstruction algorithm utilized. The point of passage is given in units of pixel pitch P of the devices accordingly (cf. section ??).

Conclusions

- Deep *understanding of sensor response* and differences between the prototypes
- New *clear concept* of the capacitive coupled clear gate as well as the reduction of the gate length showed a 36% and 81% increase in the internal gain, respectively
- Benchmark variables have been cross checked and verified
- Resolution depends on the degree of charge sharing
- Inequalities in the response of the pixels in PXD4 have been suppressed and *good homogeneity of PXD5* has been shown
- Introduction of edge contact allowed confirmation of field inhomogeneities as the cause of a reconstruction bias and allowed the reduction of *edge effect*
- Investigations of in-pixel properties showed a variation of the sensor response on the percent level
- The comparison of measured responses to model predictions allowed the *validation of the digitizer*

Overall, the DEPFET collaboration has proven that the outstanding intrinsic properties of the DEPFET sensor can successfully be implemented into a fully operational detector system with a superb signal-to-noise ratio and an excellent spatial resolution. Problems observed in previous generations have been addressed, while at the same time promising new modifications for new prototypes have been developed.

Backup

Gain Variation

Device	dir.	RMS	RMS_{adj}
STD	x	$2.5\% \pm 0.6\%$	$1.5\% \pm 0.4\%$
	y	$2.2\% \pm 1.5\%$	$1.0\% \pm 1.0\%$
HiG	x	$1.8\% \pm 1.2\%$	$1.6\% \pm 0.8\%$
	y	$3.5\% \pm 3.1\%$	$4.0\% \pm 2.2\%$
C3G	x	$2.6\% \pm 1.0\%$	$1.0\% \pm 0.7\%$
	y	$2.8\% \pm 2.5\%$	$1.7\% \pm 1.8\%$

Table 6.6: Row- and column-wise gain modulation. The RMS value represents the fluctuation in gain in x (from column to column) and in y (gain difference among the rows). The RMS_{adj} represents the fluctuation between two adjacent pixels. All values have been calculated excluding a border region of 16 pixels. The uncertainties have been obtained by bootstraping (cf. section **??**)

Comparing Position-Finding Algorithms

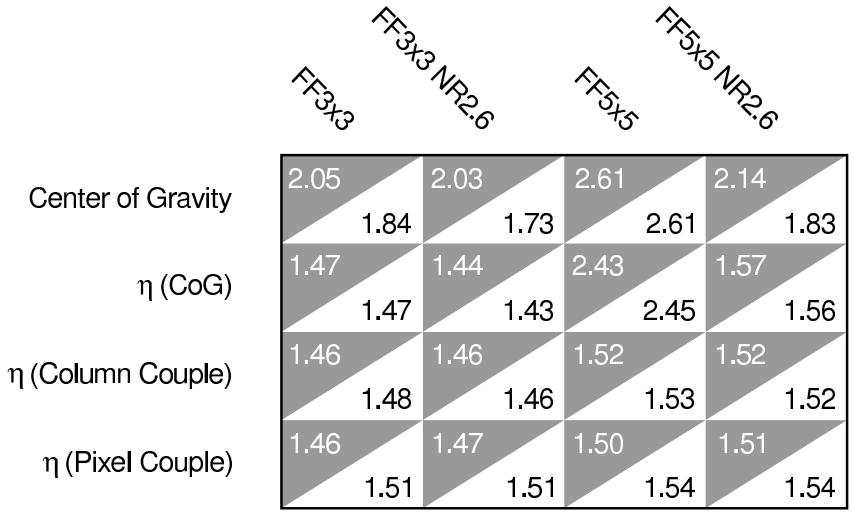

Figure 5.13: Residuals in x and y direction after hit reconstruction with different clustering methods and position-finding algorithms. Clustering is done with the fixed frame size of 3x3 and 5x5 pixel. NR2.6 denotes the rejection of signals that are below 2.6 $\times$ noise. The PFA are explained in the text. The white number on gray ground is representing the residual in x direction and the black on white number the residual in y. All numbers are in units of μm.

Upper and Lower Resolution Limit

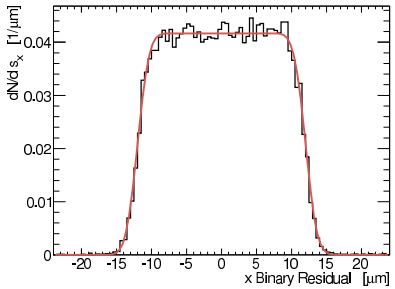

Figure 6.9: Residual of track fit and binary hit position. The smeared edges of the rectangular shape are caused by the limited telescope resolution. Calculated from STD for the x direction. For value of the one parameter (σ of faces) box fit (red line) see text.

$$PD(\Delta t) = erf\left(\frac{P/2}{\sqrt{2}\cdot\Delta t}\right) - erf\left(\frac{-P/2}{\sqrt{2}\cdot\Delta t}\right)$$

Fitting above equation to $D(b,t)$ allows the measurement of the lower telescope resolution to

$$\Delta t_l = 1.30\mu m$$

in x and

$$\Delta t_l = 1.29\mu m$$

in the y direction.

- all sensor planes are in perfect alignment
- the beam is perpendicular to the sensor planes and has no angular spread
- multiple scattering is negligible
- all sensors are equal and have the same spatial resolution Δx

$$\Delta s^2 = \Delta x^2 + 5\cdot\Delta x^2\left(\frac{1}{5}\right)^2$$

The upper telescope resolution is calculated to

$$\Delta t_u = 0.56\mu m$$

in x and

$$\Delta t_u = 0.49\mu m$$

in the y direction.